M-6

SLOW WAVE PROPAGATION IN GENERALIZED CYLINDRICAL WAVEGUIDES LOADED WITH A SEMICONDUCTOR

C. M. Krowne
Electronics Technology Division
Naval Research Laboratory, Washington, DC 20375

Abstract

For a parallel-plate waveguide and a microstrip line loaded with a semiconductor slab of resistive or active character the complex propagation constant γ is determined. γ is found for higher order branches for microwave and millimeter-wave frequencies between 10 and 140 GHz, representing a very comprehensive study of phase velocity slowing. An assessment of slowing in generalized cylindrical waveguide structures at millimeter-wave frequencies is obtained from this study.

Introduction

Slow wave structures and devices are important because of the many applications to which they have been applied and to which they may be applied in the future. Applications using an electron-electromagnetic interaction include devices such as the solid state traveling wave amplifier, solid state magnetron, distributed FET, and distributed amplifier. Applications using only the electromagnetic slowing effect include the variable phase shifter, voltage-tunable filter, delay line, and variable coupling coefficient directional coupler.

It is the intent of this paper to obtain an overall picture of the millimeter wave slowing behavior of a generalized cylindrical waveguide structure loaded with a semiconductor slab. To accomplish this task, two structures are examined, a parallel-plate waveguide and a microstrip line, both loaded by a dielectric-semiconductor two-layered medium. The complex propagation constant γ is found numerically for these two structures to determine the basic attenuation (or gain) and slowing properties for many branches of the dispersion diagram. Both resistive and active semiconductors are considered. Resistive microwave conductivities ($\sigma > 0$) may be obtained from materials like Si under low or high electric field d.c. bias conditions, where the time-harmonic electromagnetic wave is taken as a perturbation (small signal) so that the a.c. differential conductivity may be defined. At low d.c. bias conditions, $\sigma = \sigma_{ac} = \sigma_{dc}$. Active media with $\sigma < 0$ can be obtained from materials exhibiting negative a.c. differential conductivity at sufficiently high d.c. bias electric field, such as GaAs and its related ternary and quaternary alloys. High d.c. electric field, isotropic microwave $\sigma < 0$ is used in the numerical calculations to allow comparison to the low d.c. electric field, isotropic microwave $\sigma > 0$ results. This does not mean in actual practice that the high field microwave conductivity is isotropic. The tensor nature of the microwave conductivity will certainly depend on the number of orthogonally applied d.c. bias electric fields.

Other waveguide structures such as slot line, coplanar waveguide, suspended microstrip, and variants of these structures are not expected to have the physical behavior of their dispersion diagrams differ significantly from the findings of this paper, although details may differ between generalized cylindrical structures.

In the past most attention has been focused on the fundamental parallel-plate TM branch or the fundamental covered microstrip branch [1]-[6], and the fundamental coplanar line branch [7], [8], all at microwave frequencies and lower. No comprehensive study of slow wave behavior involving examination of the higher order branches at millimeter wave frequencies for lossy as well as active semiconductor media has been done. (Active media, of course, have been examined for gain behavior—see for example [9].) This paper addresses that problem.

Two-layer loaded waveguides are of special interest when the layer over the semiconductor is chosen as an insulator because the slow wave structure over the insulator is electrically isolated from the semiconductor. More specifically, this isolation allows a controlling bias to be applied to the slow wave conductor, creating a space charge depletion layer under the dielectric and as a result modulating the dielectric's effective thickness. Since the slow wave effect is due to the different partitioning of magnetic and electric energy between the layers, altering one of the layer's thickness will as a consequence change the propagating phase velocity. Besides the MIS (metal-insulator-semiconductor) slow wave structure, the variable phase velocity control quality can be obtained by creating a Schottky barrier slow wave line over a semiconductor slab. This structure is a two-layer loaded line because of the depletion layer associated with the Schottky barrier junction. The depletion layer acts as the insulating region which may be varied in thickness by a controlling bias. (There is a fundamental difference between the dielectric and depletion region, namely the static space charge in the depletion region due to the donor and acceptor dopants.) In the limit as the dielectric layer width approaches zero, noticeable slowing may still occur, although its value may be lower than that found for a finite dielectric thickness.

Results

Parallel-Plate Waveguide

Figure 1 shows a cross-sectional diagram of the parallel-plate waveguide structure. Medium 1 has thickness $b_1 = y_1$, complex permittivity ϵ_1', and complex permeability μ_1'. Medium 2 has thickness $b_2 = -y_2$, complex permittivity ϵ_2', and complex permeability μ_2'.

Figures 2-5 give the $\gamma (= \alpha + j\beta)$ results as $\bar{\beta}$ (normalized to free space value) and α (attenuation) versus f plotted in each figure. Muller's method [10] is used to determine the $\bar{\gamma} = \bar{\gamma}_n$ eigenvalue solutions where $n = 0, 1, 2, \ldots$ indicates the particular branch ordered according to decreasing $\bar{\beta}$, $n = 0$ being the lowest or fundamental branch with the largest slowing factor $\bar{\beta}$. The notation for n agrees with [1] for TM_z in the $\sigma = 0$ limit where $n = 0$ is the quasi-TEM case. For illustrative purposes and to allow comparison to the fundamental mode results in [1] (agreement with their Fig. 3 results is within 5%), the $\sigma > 0$ calculations are done here for $\epsilon_{r1} = 4.5$, $\epsilon_{r2} = 12$, $b_1 = 0.3\ \mu$m, $b_2 = 190\ \mu$m, and $\sigma = 10^3 \mho/$m. The nominal values of ϵ_{ri} chosen could represent SiO_2-Si layers.

Results are given for 10 GHz $\leq f \leq$ 140 GHz. The un-normalized attenuation constant α in Figs. 2 and 3 increases gently with f. Slowing factor $\bar{\beta}$ decreases as n increases, the reverse trend as seen for α. The change in slowing $\Delta\bar{\beta}/\bar{\beta}$ over the 10 to 140 GHz range decreases as n increases for TM_z. Such behavior is only observable for the $n = 0$ TE_z branch which has a 34.3% change, the other branches exhibiting little change over f in comparison. Comparison of the TM_z and TE_z results (same n) show that $\bar{\beta}$ is significantly larger for TM_z and that α is larger for TE_z, these differences being especially apparent at lower f.

Figures 4 and 5 graph the γ results for $\sigma < 0$, with values of $\epsilon_{r1} = \epsilon_{r2} = 12$, $b_1 = 0.3\ \mu$m, $b_2 = 200\ \mu$m, and $\sigma = -10^3 \mho/m$ having been chosen. Nominal values of ϵ_{ri} could correspond to depleted GaAs-GaAs layers. The behavior of the TM_z and TE_z results for an active medium semiconductor are similar to the resistive medium behavior (Figs. 2 and 3) in that $\bar{\beta}$ and α for $\sigma > 0$ and $\bar{\beta}$ and $-\alpha$ for $\sigma < 0$ have similar dependences on n and f. One important difference is that $\bar{\beta}$ does not necessarily increase with increasing n at lower $f (f \lessapprox 40$ GHz), this effect being due to differing ϵ_{r1} and b_2. The second major difference is that for an excitation involving several TM_z and TE_z modes, when $\sigma > 0$ the lowest n branch will be favored due to attenuation, whereas for $\sigma < 0$ the higher n branches could become dominant as their gain causes a larger difference in wave growth over the lower n branches. It is interesting to note that $\gamma(\sigma < 0) = \alpha(\sigma < 0) + j\beta(\sigma < 0) = -\alpha(\sigma > 0) + j\beta(\sigma > 0)$. Thus the results in Figs. 4 and 5 can also represent the depleted GaAs — GaAs layer results for positive microwave conductivity with low d.c. field bias.

Microstrip Line

Figure 6 shows a cross-sectional drawing of the partially open microstrip structure. It has besides the basic geometry seen in Fig. 1,

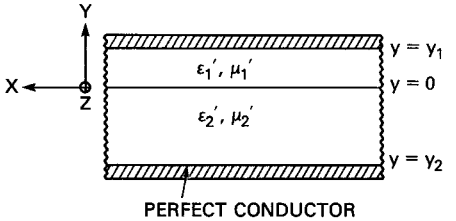

Fig. 1: Cross section of two medium loaded parallel-plate waveguide

0149-645X/83/0000-0187 $01.00 © 1983 IEEE

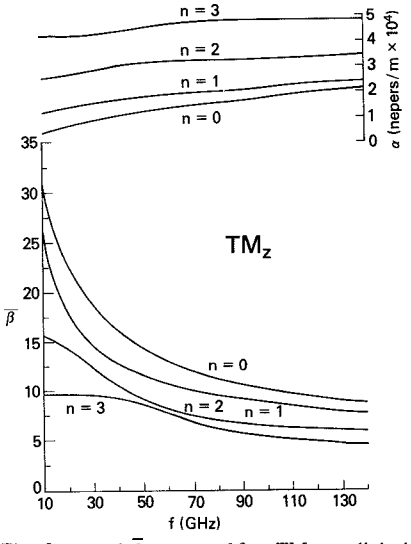

Fig. 2: α and $\bar{\beta}$ versus f for TM_z parallel-plate modes. $\epsilon_{r1} = 4.5$, $\epsilon_{r2} = 12$, $b_1 = 0.3\ \mu$m, $b_2 = 190\ \mu$m, and $\sigma = 10^3 \mho/m$.

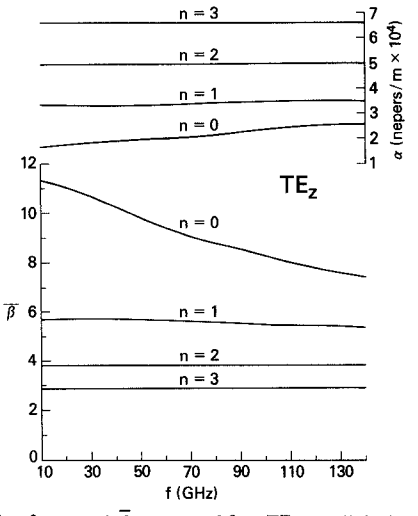

Fig. 3: α and $\bar{\beta}$ versus f for TE_z parallel-plate modes. Same parameters used as in Fig. 2 where $\sigma > 0$.

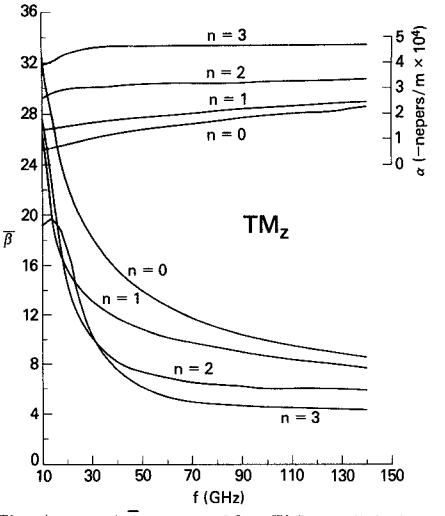

Fig. 4: α and $\bar{\beta}$ versus f for TM_z parallel-plate modes. $\epsilon_{r1} = \epsilon_{r2} = 12$, $b_1 = 0.3\ \mu$m, $b_2 = 200\ \mu$m, and $\sigma = -10^3 \mho/m$.

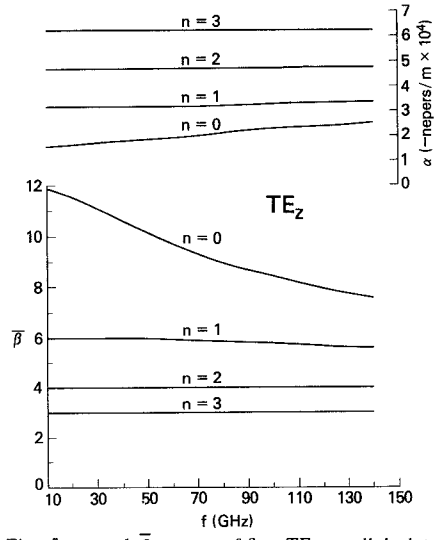

Fig. 5: α and $\bar{\beta}$ versus f for TE_z parallel-plate modes. Same parameters as in Fig. 4 where $\sigma < 0$.

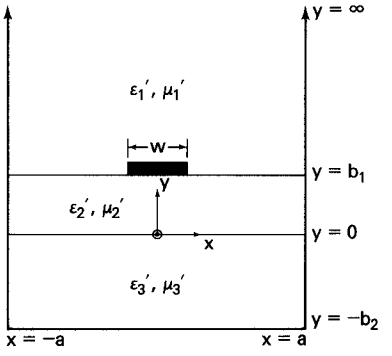

Fig. 6: Cross section of partially open microstrip line

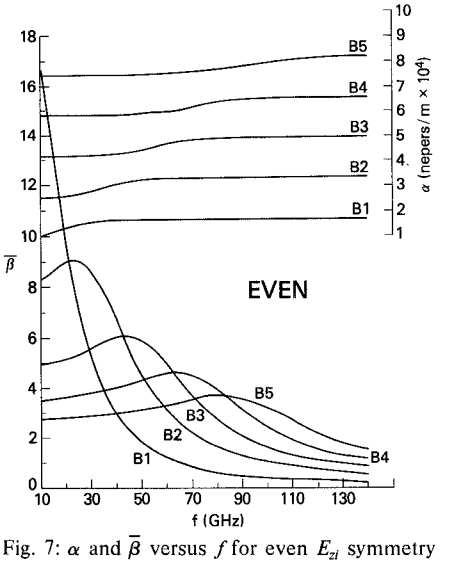

Fig. 7: α and $\bar{\beta}$ versus f for even E_{zi} symmetry microstrip line modes. $\epsilon_{r1} = 4.5$, $\epsilon_{r2} = 12$, $b_1 = 0.3\ \mu$m, $b_2 = 190\ \mu$m, $a = 5000\ \mu$m, $w = 1000\ \mu$m, and $\sigma = 10^3 \mho/m$.

electric walls placed at $x = \pm a$. These walls allow the use of a discrete Fourier transform method enabling the current distribution on the microstrip line ($|x| \leqq w/2$) and the fields to be approximately constructed from a finite sum of L terms for the x dependence. Because the dispersion results are not overly sensitive to the particular choice of current basis functions, and to maintain simplicity, $J_z(x)$ and $J_x(x)$ are constructed using one basis function apiece. These basis functions are $J_{z1}(x) = 1/w$, $J_{x1}(x) = (-j/\pi w)\sin(2\pi x/w)$ for even modes and $J_{z1}(x) = -2jx/w^2$, $J_{x1}(x) = (2/\pi w)\cos(\pi x/w)$ for odd modes when $|x| \leqq w/2$ and zero otherwise. The field solution using a hybrid mode approach [11], [12] for the microstrip problem is decomposed into two parts, the solution giving $E_{zi}(x, y)$ with even x symmetry and the solution giving E_{zi} with odd x symmetry.

The validity of the $N = M = 1$ single basis function analysis (the basis sets are generally J_{zi}, $i = 1, \cdots, N$ and J_{xm}, $m = 1, \cdots, M$) is supported by using orthogonal complete basis sets ($I = N = M$) and comparing the results for differing I and L to the particular single basis function choice above. The complete sets used are $J_{zi}(x) = \cos[2x\pi(i-1)/w]/\sqrt{1-(2x/w)^2}$, $J_{xi}(x) = \sin(2x\pi i/w)/\sqrt{1-(2x/w)^2}$ for even modes and $J_{zi}(x) = \sin[x\pi(2i-1)/w]/\sqrt{1-(2x/w)^2}$, $J_{xi}(x) = \cos[x\pi(2i-1)/w]\sqrt{1-(2x/w)^2}$ for odd modes. Good agreement between these approaches is found. For example, using $I = 3$, $L = 300$ for the complete sets makes the single basis function approach and the complete basis function approach agree within $(\Delta\alpha, \Delta\beta) \leqq (1\%, 2\%)$.

To allow comparison of the numerical results to follow in this section to those in Figs. 2-5, the microstrip parameters are set to $\epsilon_{r1} = 4.5$, $b_2 = 190\ \mu$m, $a = 5000\ \mu$m, $w = 1000\ \mu$m, and $\sigma = 10^3 \mho/m$ (medium 3) for the $\sigma > 0$ case. For $\sigma < 0$, $\epsilon_{r1} = \epsilon_{r2} = 12$, $b_1 = 0.3\ \mu$m, $b_2 = 200\ \mu$m, $a = 5000\ \mu$m, $w = 1000\ \mu$m, and $\sigma = -10^3 \mho/$m. Let us consider the $\sigma > 0$ case first.

L is set to 30 terms (except for branch B1 where $L = 100$) in Fig. 7 and 100 in Fig. 8 for respectively the even and odd modes. Beyond about $L = 30$ the even mode results are relatively insensitive to additional terms (the effect is on the order of 1% or less) whereas for the odd modes this insensitivity begins at larger L so $L = 100$ is chosen.

Figures 7 and 8 demonstrate (5 branches B1-B5 are plotted) the change in γ going from a closed structure such as the parallel-plate waveguide (Fig. 1) to the partially open structure such as the microstrip line (Fig. 6). Although for low frequencies $f \lesssim 20$ GHz decreasing $\bar{\beta}$ of the branches $B1$, $B2$ ... corresponds to increasing α (as in Figs. 2 and 3), this progression is disrupted at higher frequencies, for example at 70 GHz. The progression is reversed beyond 90 GHz for the branches $B1 - B5$, but this trend is not necessarily true for the other higher order modes not plotted in the figures. What appears to be occurring is that at high frequencies, say 90 GHz, the $B1$ branch wave is being guided significantly by the (open air space)-layers combination. A surface wave is brought into existence which samples appreciably the air environment with some of the electromagnetic field energy lying above the $y = b_1$ interface. The effect is not as large for the $B2$ branch wave relative to

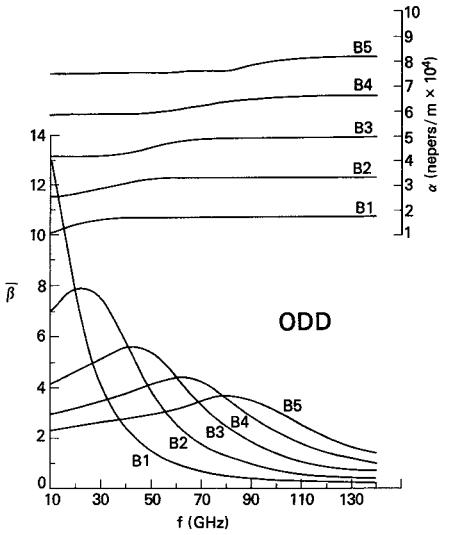

Fig. 8: α and $\bar{\beta}$ versus f for odd symmetry microstrip line modes. Same parameters used in Fig. 7 where $\sigma > 0$.

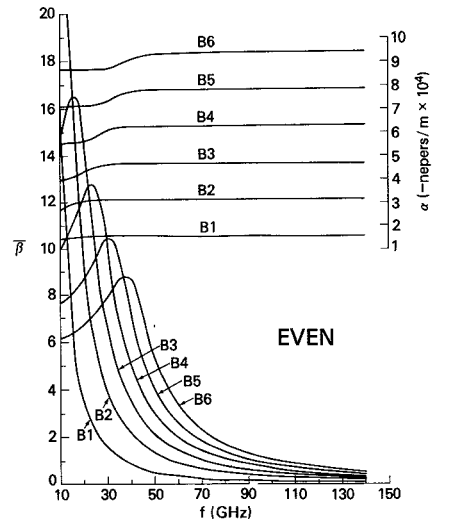

Fig. 9: α and $\bar{\beta}$ versus f for even symmetry microstrip line modes. $\epsilon_{r1} = \epsilon_{r2} = 12$, $b_1 = 0.3\ \mu$m, $b_2 = 200\ \mu$m, $a = 5000\ \mu$m, $w = 1000\ \mu$m, and $\sigma = -10^3 \mho/m$.

the $B1$ branch wave at 90 GHz, therefore its $\bar{\beta}_2 > \bar{\beta}_1$. Such an argument explains the results in Figs. 7 and 8.

Comparing the microstrip line results below 20 GHz to the parallel-plate results suggests an averaging of the TM_y and TE_y $\bar{\beta}$ values in Figs. 2 and 3 according to $<\bar{\beta}> \cong (\bar{\beta}_{TM} + \bar{\beta}_{TE})/3$. Averaging above 20 GHz is not as obvious to identify by such a simple expression. Averaging of the transverse modes makes sense on a physical basis because the microstrip analysis requires a hybrid mode approach. The averaging effect is also seen in the α results. Comparison of Figs. 3 and 7 shows that $\alpha_{TE} \geqq \alpha_M$, the effect becoming most noticeable for branches B_i and $n = i - 1$ with small i, suggesting the averaging in of the TM_y behavior to varying degrees depending on the frequency and branch.

The even and odd mode results differ much more in $\bar{\beta}$ than α, the α differences being small. $\bar{\beta}$ differences can be as large as 25% if branch peaks are compared.

Even mode $\sigma < 0$ results are given in Fig. 9 using $L = 30$ terms. The behavior of γ for $\sigma < 0$ is very similar to the $\sigma > 0$ results. Again one notices an averaging effect, tending to favor the TE_y over the TM_y modes (of Figs. 4 and 5) when combining to form the hybrid mode solution. $|\alpha_{TE}| \geqq |\alpha_M|$ beyond about 50 GHz. Comparison of the $\sigma < 0$ (Fig. 9) and $\sigma > 0$ (Fig. 7) results makes clear that the $\bar{\beta}$ curves for $\sigma < 0$ are much closer and more sharply peaked when examining the branches B_i, $i \geqq 2$. The peaks, for corresponding $\bar{\beta}$ branch curves of the $\sigma > 0$ and $\sigma < 0$ results, are much larger for the $\sigma < 0$ case, the difference being as much as 2.8:1. The difference between the Fig. 7 and Fig. 9 results is due differing ϵ_{r1} and b_2. Again as for Figs. 4 and 5, Fig. 9 can represent the depleted GaAs—GaAs layer propagation constant for positive microwave conductivity if $\alpha(\sigma < 0)$ is replaced by $-\alpha(\sigma < 0) = \alpha(\sigma > 0)$.

Discussion

Open waveguide structures considerably reduce the slowing $\bar{\beta}$ in relation to a closed structure as demonstrated here by the microstrip line and parallel-plate numerical data. The data shows that the $\bar{\beta}$ reduction becomes more severe as frequency and branch number are increased. If $\bar{\beta} = 8$ is taken as a measure of adequate or sizeable slowing, then this value is attained (or exceeded) over the entire 10 to 140 GHz range by the first two parallel-plate TM_z mode branches with either $\sigma > 0$ or $\sigma < 0$. Only the first TE_z branch satisfies $\bar{\beta} \geqq 8$ for either $\sigma > 0$ or $\sigma < 0$, but only up to $f \approx 110$ GHz.

These results show, at least for the open microstrip line, that $\bar{\beta}$ won't exceed 8 beyond about 40 GHz. $\sigma = 10^3 \mho/m$ was chosen as a calculation value because evidence indicates a maximization of the slowing effect in the $10^3 < \sigma < 10^4 \mho/m$ interval. Note that for $\sigma > 0$, this σ value corresponds to a donor doping density N_D of 7.0×10^{16} cm^{-3} and 1.8×10^{16} cm^{-3} for respectively Si and GaAs at room temperature. One expects by the proper choice of geometric parameters and σ to be able to increase $\bar{\beta}$ above the numerical data reported here for some of the branches. Correctness of this supposition can be tested by calculating $\bar{\beta}$ at 100 GHz for the parallel-plate waveguide using the following parameters: $\epsilon_{r1} = \epsilon_{r2} = 12.8$, $b_1 = 0.3\ \mu$m, $b_2 = 25\ \mu$m, and $\sigma = 6 \times 10^3 \mho/m$. Such parameters could correspond to a GaAs sample at room temperature with $N_D = 1.2 \times 10^{17}$ cm^{-3}. $\bar{\beta}$ increased from 10.16 (Fig. 2) to 20.97 with a 10.4% increase in α to 1.96×10^4 nepers/m. The approximately 2:1 increase in $\bar{\beta}$ is due to the increased σ value and decreased geometric parameter b_2 value. Changing ϵ_{r1} and ϵ_{r2} (Fig. 2) to the GaAs relative dielectric constant causes α and $\bar{\beta}$ to change by respectively 6.6% and -2.2%—this is a smaller effect (comparison made with $b_2 = 190\ \mu$m).

Although the $\bar{\beta}$ increase due to a change in parameters is impressive for the parallel-plate waveguide at 100 GHz, the open microstrip numerical data seen here suggest that a 2:1 factor increase in $\bar{\beta}$ would be insufficient to place $\bar{\beta}$ above 8. A closed structure such as a parallel-plate waveguide, which properly contains and controls the distribution of electromagnetic energy, is much more amenable toward obtaining large $\bar{\beta}$ values than an open microstrip structure.

References

[1] H. Guckel, P.A. Brennan, and I. Palocz, "A parallel-plate waveguide approach to micro-miniaturized, planar transmission lines for integrated circuits," IEEE Trans. Micro. Th. Tech., Vol. MTT-15, pp. 468-476, Aug. 1967.

[2] H. Hasegawa, M. Furukawa, and H. Yanai, "Properties of microstrip line of Si-SiO_2 system," IEEE Trans. Micro. Th. Tech., Vol. MTT-19, pp. 869-881, Nov. 1971.

[3] J.M. Jaffe, "A high-frequency variable delay line," IEEE Trans. Electron Dev., Vol. ED-19, pp. 1292-1294, Dec. 1972.

[4] D. Jaeger and W. Rabus, "Bias-dependent phase delay of Schottky contact microstrip line," Electron. Lett., Vol. 9, pp. 201-203, May 1973.

[5] G.W. Hughes and R.M. White, "Microwave properties of nonlinear MIS and Schottky-barrier microstrip," IEEE Trans. Electron Dev., Vol. ED-22, pp. 945-956, Oct. 1975.

[6] P. Kennis and L. Faucon, "Rigorous analysis of planar MIS transmission lines," Electron. Lett., Vol. 17, pp. 454-456, June 1977.

[7] R. Sorrentino and G. Leuzzi, "Full-wave analysis of integrated transmission lines on layered lossy media," Electron. Lett., Vol. 18, pp. 607-608, July 1982.

[8] Y. Fukuoka and T. Itoh, "Analysis of slow-wave phenomena in coplanar waveguide on a semiconductor substrate," Electron. Lett., Vol. 18, pp. 589-590, July 1982.

[9] D.B. Matthews and J. Frey, "Growth of electromagnetic waves on the surface of a negative differential conductance material," J. Appl. Phys., Vol. 43, pp. 4981-4987, Dec. 1972.

[10] C.F. Gerald, Applied Numerical Analysis. Reading, Mass.: Addison-Wesley, 1978, p. 429.

[11] T. Itoh and R. Mittra, "Spectral-domain approach for calculating the dispersion characteristics of microstrip lines," IEEE Trans. Micro. Th. Tech., Vol. MTT-21, pp. 496-499, July 1973.

[12] T. Itoh and R. Mittra, "A technique for computing dispersion characteristics of shielded microstrip lines," IEEE Micro. Th. Tech., Vol. MTT-22, pp. 896-898, Oct. 1974.